RePOSE: Real-Time Iterative Rendering and Refinement for 6D Object Pose Estimation

Shun Iwase¹ Xingyu Liu¹ Rawal Khirodkar¹ Rio Yokota² Kris M. Kitani¹

Carnegie Mellon University ²Tokyo Institute of Technology

Abstract

The use of iterative pose refinement is a critical processing step for 6D object pose estimation, and its performance depends greatly on one's choice of image representation. Image representations learned via deep convolutional neural networks (CNN) are currently the method of choice as they are able to robustly encode object keypoint locations. However, CNN-based image representations are computational expensive to use for iterative pose refinement, as they require that image features are extracted using a deep network, once for the input image and multiple times for rendered images during the refinement process. Instead of using a CNN to extract image features from a rendered RGB image, we propose to directly render a deep feature image. We call this deep texture rendering, where a shallow multi-layer perceptron is used to directly regress a view invariant image representation of an object. Using an estimate of the pose and deep texture rendering, our system can render an image representation in under 1ms. This image representation is optimized such that it makes it easier to perform nonlinear 6D pose estimation by adding a differentiable Levenberg-Marquardt optimization network and back-propagating the 6D pose alignment error. We call our method, RePOSE, a Real-time Iterative Rendering and Refinement algorithm for 6D POSE estimation. RePOSE runs at 71 FPS and achieves state-of-the-art accuracy of 51.6% on the Occlusion LineMOD dataset - a 4.1% absolute improvement over the prior art, and comparable result on the YCB-Video dataset with a much faster runtime.

1. Introduction

State-of-the-art 6D object pose estimation methods use iterative refinement to align an input image of an object against a template image (*e.g.*, 3D rendering of that object), but the performance of alignment depends heavily on the feature space in which the two images are compared. Iterative refinement methods repeatedly adjust a set of transformation parameters to generate a sequence of template images (*e.g.*, via image warping or rendering) to be matched

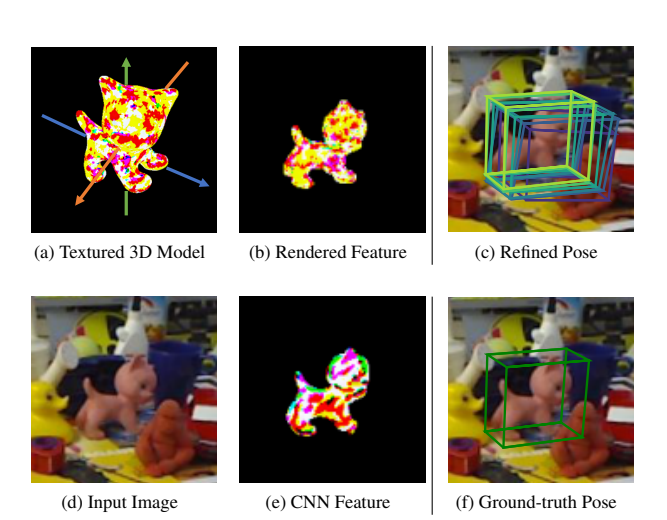


Figure 1: **RePOSE Framework:** (a) 3D model with deep texture is projected to obtain (b) the rendered image representation. (c) The pose is refined iteratively by minimizing the projection error of the rendered image representation and (e) the CNN feature extracted from (d) the input image.

against an input image. When the template image and input image become aligned, the final transformation parameters describe the pose of the object in the input image. One's choice of feature space for image alignment has a significant impact on both accuracy and speed.

Classical image alignment algorithms estimate the transformation between two images using photometric error but they can fail under diverse illumination or gross pose differences. Non-linear least squares methods such as inverse compositional image alignment or active appearance models are extremely efficient but straightforward implementations of such methods can be unstable under significant illumination or pose changes.

Deep image feature based image alignment algorithms use a convolutional neural network (CNN) to define a deep convolutional feature space in which to match images, resulting in methods that are more robust to illumination and pose variation. Recent work [23, 10, 14, 17, 30] has shown

a remarkable performance by combining a deep neural network for coarse pose estimation followed by a CNN-based iterative pose optimization process. Unfortunately, CNN-based methods tend to have low speed performance since CNN features must be extracted many times during the refinement step. There is a need to develop refinement-based 6D object pose estimation algorithms which are both robust and efficient.

The main technical insight presented in this work is that one can learn an image feature representation which is both robust for alignment and efficient to compute. As stated earlier, the main bottleneck of deep feature-based refinement methods is that the deep feature must be extracted repeatedly during the refinement process. To bypass this bottleneck, we show that it is possible to directly render deep features using a graphics render. The rendering process decouples the shape of an object from the texture of the object. At the time of rendering, texture is mapped to the 3D shape and then projected as a 2D image. Instead of mapping an RGB valued texture to the object, we can alternatively render a deep feature texture to the object. Then the rendered object can then be directly aligned to the deep features of the input image. By retaining the deep feature representation during rendering, the pose alignment is robust and the refinement process becomes very efficient.

We call our method, RePOSE, a <u>Re</u>al-time Iterative <u>Re</u>ndering and <u>Re</u>finement algorithm for 6D <u>POSE</u> estimation. RePOSE refines an object pose by minimizing the distance between the deep features of the input and a rendered deep feature image. Since the input image is fixed during iterative refinement, its feature is only computed once using a CNN. In contrast, the deep features of the template image are directly generated using computer graphics rendering. The rendering process takes less than a millisecond which greatly increases the speed of the iterative refinement process. The deep feature representation is learned such that nonlinear optimization can be easily performed through a differentiable Levenberg-Marquardt optimization network [15].

We evaluate RePOSE on three popular 6D object estimation datasets - LineMOD [9], the challenging Occlusion LineMOD [2], and YCB-Video [29]. RePOSE sets a new state of the art on the Occlusion LineMOD (51.6%) [2] dataset and achieves comparable performance on the other datasets with a much faster runtime (71FPS). Additionally, we perform ablations to validate the effectiveness of our proposed deep texture rendering and refinement network over prior work.

2. Related Work

Two-stage pose estimation methods Recently, PVNet [17], DPOD [30], and HybridPose [23] have shown excel-

lent performance on 6D object pose estimation using a twostage pipeline to estimate a pose: (i) estimating a 2D representation (e.g. keypoints, dense correspondences, edge vectors, symmetry correspondences), (ii) PnP algorithm [13, 6] for pose refinment. DOPE [26] and BB8 [18] estimate the corners of the 3D bounding box and refine it using a PnP algorithm. Instead of regarding the corners as keypoints, PVNet [17] places the keypoints on the object surface via the farthest point sampling algorithm. PVNet also shows that their proposed voting-based keypoint detection algorithm is effective especially for occluded objects. Hybrid-Pose [23] uses multiple 2D representations including keypoints, edge vectors, and symmetry correspondences and demonstrates superior performance through constraint optimization. DPOD [30] takes advantage of the dense correspondences using a UV map as a 2D representation. However, since the PnP algorithm is sensitive to small errors in the 2D representation, it is still challenging to estimate the object pose especially under occlusion. RePOSE uses PVNet [17] as the initial pose estimator using the official implementation.

Pose refinement networks Instead of using an algorithm like PnP, recent works [29, 24, 30, 23, 14] have demonstrated that using a pose refinement network after the initial pose estimator is effective for 6D object pose estimation. For practical applications, due to its iterative nature, the runtime of the pose refinement network is crucial. PoseCNN [29] and AAE [24] use an ICP algorithm [31] using depth information to refine the pose with a runtime of around 200 ms. SSD6D [10] and HybridPose [23] proposed to refine the pose by optimizing a modification of reprojection error. DeepIM [14], DPOD [30], and CosyPose [12] introduce a deep learning-based refinement network using the cropped input image and a rendered object image. Their methods require a high-quality texture map of a 3D model to compare the images. However, it is still challenging to obtain accurate texture scans of metalic or transparent objects. NeMO [28] proposes a pose refinement method using the standard differentiable rendering and learning the texture of a 3D model via contrastive loss. However, gradient descent is used for optimization, and thus, it takes more than 8s for inference and is not fast enough for real-time applications.

Non-linear least squares optimization Non-linear least squares optimization is a widely research topic in machine learning. In computer vision, it is often used to find an optimal pose which minimizes the reprojection error or photometric error [1, 16, 22]. Recently some works [25, 27] incorporate non-linear least square algorithms like Gauss-Newton and Levenberg-Marquardt [15] into a deep learning network for efficient feature optimization in VisualSLAM.

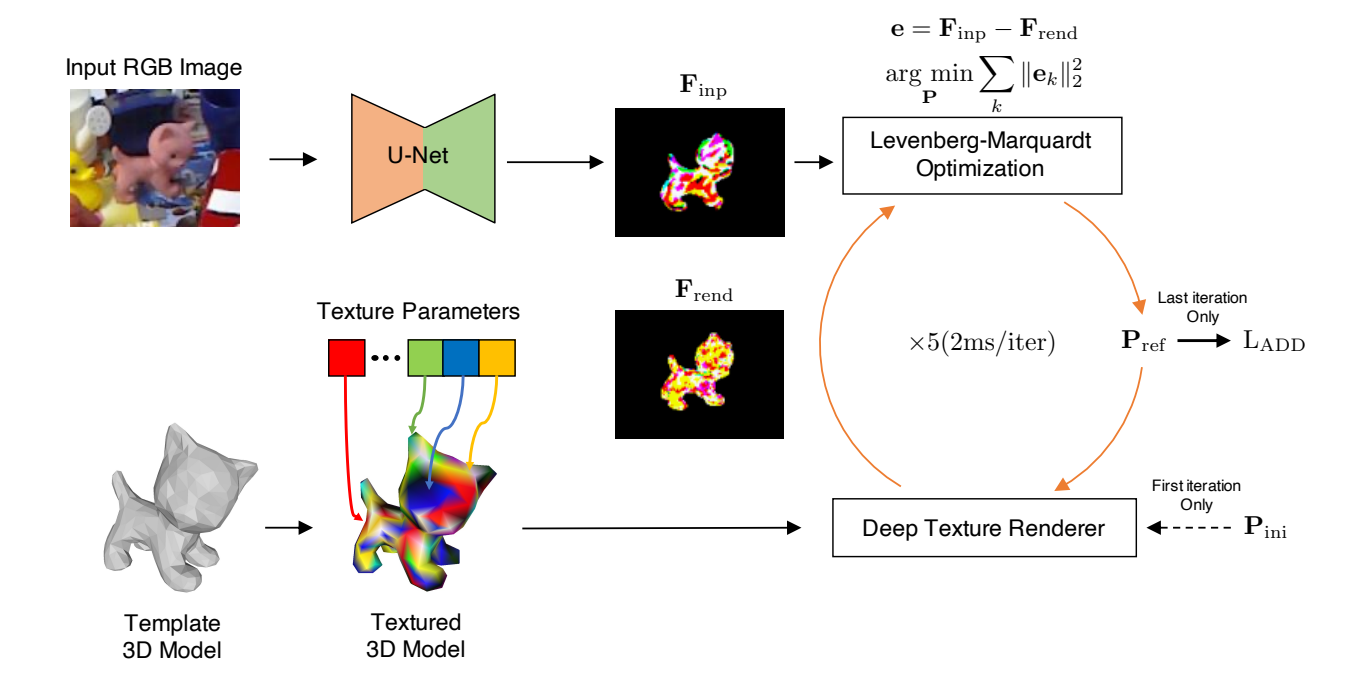


Figure 2: Overview of the RePOSE refinement network. Given an input image I and the template 3D model M with deep textures, U-Net and deep texture renderer output features \mathbf{F}_{inp} and \mathbf{F}_{rend} respectively. We use Levenberg-Marquardt optimization [15] to obtain the refined pose \mathbf{P}_{ref} . The refined pose \mathbf{P}_{ref} after 5 iterations is used to compute the loss $L_{ADD(-S)}$. The decoder of U-Net and deep textures (seed parameters, and fc layers) are trained to minimize $L_{ADD(-S)}$ and L_{diff} .

RePOSE is inspired by similar formulation as in [25] which helps us achieve real-time performance. Additionally, iteratively reweighted least squares (IRLS) [8] was used to reduce the effect of outliers. Similarly, functions like Huber, Cauchy, Geman-McClure are generally used to weigh per pixel errors. RePOSE adopts the IRLS with Cauchy function to compute the distance between pixel level features.

3. RePOSE: Real-time Pose Refinement

Given an input image I with an object with pose \mathbf{P}_{gt} and the template 3D model \mathcal{M} , RePOSE predicts pose $\hat{\mathbf{P}}$ of model \mathcal{M} which matches \mathbf{P}_{gt} in I. We extract a feature \mathbf{F}_{inp} from image I using a CNN Φ *i.e.* $\mathbf{F}_{inp} = \Phi(\mathbf{I})$. RePOSE then refines the initial pose estimate $\mathbf{P}_{ini} = \Omega(\mathbf{I})$ where Ω is any pose estimation methods like PVNet [17] and PoseCNN [29] in real time using differentiable Levenberg-Marquardt (LM) optimization [15]. RePOSE renders the template 3D model with learnable deep textures in pose P to extract feature \mathbf{F}_{rend} . The pose refinement is performed by minimizing the distance between \mathbf{F}_{inp} and \mathbf{F}_{rend} . We now describe in detail (1) \mathbf{F}_{inp} extraction, (2) \mathbf{F}_{rend} extraction and finally (3) the pose refinement using LM optimization.

3.1. Feature Extraction of an Input Image F_{inp}

We adapt a U-Net [19] architecture for the CNN Φ . The decoder outputs a deep feature map for every pixel in I. The per pixel feature $\mathbf{F}_{\text{inp}} \in \mathbb{R}^{w \times h \times d}$ is extracted by the decoder. Figure 1 (b) provides a visual illustration of \mathbf{F}_{inp} extracted from the input image I. Note that the channel depth d is a flexible parameter but we found d=3 to be optimal. The pre-trained weights of PVNet [17] or PoseCNN [29] are used for the encoder and only the decoder is trained while training RePOSE.

3.2. Template 3D Model Rendering F_{rend}

The template 3D model \mathcal{M} with pose $\mathbf{P} = \{\mathbf{R}, \mathbf{t}\}$ where \mathbf{R} is 3D rotation and \mathbf{t} is 3D translation, is projected to 2D to render the feature \mathbf{F}_{rend} . Let the template 3D model $\mathcal{M} = \{\mathcal{V}, \mathcal{C}, \mathcal{F}\}$ be represented by a triangular watertight mesh consisting of N vertices $\mathcal{V} = \{V_n\}_{n=1}^N$ where $V_n \in \mathbb{R}^3$, faces \mathcal{F} and deep textures \mathcal{C} . V_n is the 3D coordinate of the vertex in the coordinate system centered on the object. Each vertex V_n has a corresponding vertex deep texture $\mathbf{C}_n \in \mathbb{R}^d$, $\mathcal{C} = \{\mathbf{C}_n\}_{n=1}^N$, which is learned. Note that the dimensions of the vertex deep texture d must match depth dimension of input image feature \mathbf{F}_{inp} so that they can be compared during alignment.

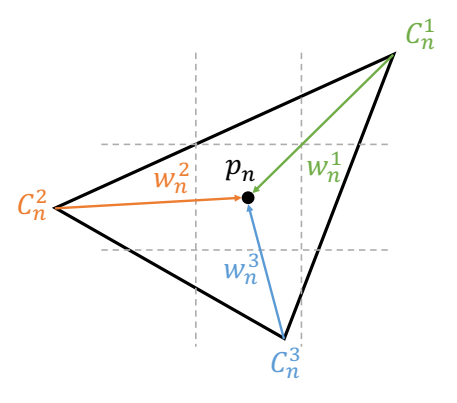


Figure 3: Rasterization of deep textures into a pixel p_n as the weighted sum of \mathbf{C}_n^i using w_n^i as weights in the barycentric coordinate system, $\sum_i^3 w_n^i = 1$.

RePOSE projects the 3D mesh onto to the image plane using a pinhole camera projection function π (homogeneous to inhomogeneous coordinate conversion). Specifically, we map the vertex \mathbf{V}_n to $\mathbf{v} \in \mathbb{R}^2$ using eq 1.

$$\mathbf{v}_n = \pi \left(\mathbf{V}_n \mathbf{R}^\top + \mathbf{t}^\top \right) \ \forall \ n \tag{1}$$

The vertex deep textures $\mathbf{C}_n \in \mathbb{R}^3$ are learnable and computed using a 2-layer fully-connected network. The deep texture at each pixel is calculated by rasterization using the deep textures \mathbf{C}_n in barycentric coordinates w as shown in Figure 3. This operation can be parallelized using a GPU and our custom implementation takes less than 1 ms to render $\mathbf{F}_{\text{rend}}(x,y)$ at a pixel location (x,y) is computed as follows:

$$\mathbf{F}_{\text{rend}}(x,y) = \sum_{i=1}^{3} w_n^i C_n^i \tag{2}$$

where the triangular face index n corresponding to the pixel p_n at (x,y) is found by ray tracing and w_i is the normalized barycentric weight corresponding to the coordinates (x,y) inside the triangle (Figure 3). Simply put, the rendered deep feature $\mathbf{F}_{\text{rend}}(x,y)$ is a linear combination of deep textures of the three projected vertices.

 $\mathbf{F}_{\mathrm{rend}}$ is end-to-end learnable by backpropagation. The gradient of $\mathbf{F}_{\mathrm{rend}}$ with respect to the three deep textures of the triangle $\{C_n^i\}_{i=1}^3$ is as follows:

$$\frac{\partial \mathbf{F}_{\text{rend}}(x,y)}{\partial C_n^i} = w_n^i. \tag{3}$$

Note that \mathbf{F}_{rend} is the output of a non-linear function Ψ of the template 3D model \mathcal{M} and it's pose \mathbf{P} , *i.e.*, $\mathbf{F}_{rend} = \Psi(\mathbf{P}, \mathcal{M})$ where Ψ is the deep texture renderer (Figure 2).

3.3. Levenberg-Marquardt Optimization

After computing \mathbf{F}_{inp} (Section 3.1) and \mathbf{F}_{rend} (Section 3.2), the optimal pose $\hat{\mathbf{P}}$ is calculated by minimizing the following objective function:

$$\mathbf{e} = \text{vec}(\mathbf{F}_{\text{inp}}) - \text{vec}(\mathbf{F}_{\text{rend}}),$$
 (4)

$$\hat{\mathbf{P}} = \underset{\mathbf{P}}{\operatorname{arg\,min}} \sum_{k} ||e_k||_2^2,\tag{5}$$

where e_k denotes the k^{th} element of the error $\mathbf{e} \in \mathbb{R}^{whd}$ and is the element-wise difference between the flattened values of \mathbf{F}_{inp} and \mathbf{F}_{rend} . To perform optimization efficiently, we only use the error \mathbf{e} in the pixel where the mask of \mathbf{F}_{inp} exists.

We solve this non-linear least squares problem using the iterative Levenberg-Marquardt (LM) algorithm. The update rule for the pose ${\bf P}$ is as follows:

$$\Delta \mathbf{P} = (\mathbf{J}^T \mathbf{W} (\mathbf{e}) \mathbf{J} + \lambda \mathbf{I})^{-1} \mathbf{J}^T \mathbf{W} (\mathbf{e}) \mathbf{e}, \qquad (6)$$

$$\mathbf{P}_{i+1} = \mathbf{P}_i + \Delta \mathbf{P},\tag{7}$$

where **J** is the Jacobian of the objective with respect to the pose **P**, **W** (e) is a diagonal matrix of weights, and λ is a learnable step size.

The Jacobian **J** can be decomposed as:

$$\mathbf{J} = \frac{\partial \mathbf{F}_{\text{rend}}}{\partial \mathbf{P}} = \frac{\partial \mathbf{F}_{\text{rend}}}{\partial \mathbf{x}} \frac{\partial \mathbf{x}}{\partial \mathbf{P}}$$
(8)

where \mathbf{x} is a vector of all 2D image coordinate. We compute $\frac{\partial \mathbf{F}_{\text{rend}}}{\partial \mathbf{x}}$ using a finite difference approximation and $\frac{\partial \mathbf{x}}{\partial \mathbf{P}}$ is computed analytically. Please refer supplemental for the details. The diagonal elements of the weight matrix $\mathbf{W}(\mathbf{e})$ are parametrized with a Cauchy function:

$$\mathbf{W}(\mathbf{e})[k,k] = \frac{1}{1 + (e_k/\gamma)^2},$$
 (9)

where γ is a learnable parameter. We roll out the gradient updates for a fixed number of iterations to estimate all the LM parameters (λ, γ) during the refinement process.

We minimize a loss function $\mathcal{L}_{ADD(-S)}$ based on the ADD(-S) score:

$$\mathcal{L}_{\text{ADD(-S)}} = S_{\text{ADD(-S)}}(\mathbf{P}, \mathbf{P}_{\text{gt}}) \tag{10}$$

where S is the function used to calculate the distance used in the ADD(-S) score. Additionally, we also minimize a loss function $\mathcal{L}_{\text{diff}}$ which ensures the value of the objective function is minimized when the pose \mathbf{P} is equal to \mathbf{P}_{gt} :

$$e^{gt} = vec(\mathbf{F}_{inp}) - vec(\Psi(\mathbf{P}_{gt}, \mathcal{M})),$$
 (11)

$$\mathcal{L}_{\text{diff}} = \sum_{k} ||\mathbf{e}_{k}^{\text{gt}}||_{2}^{2}. \tag{12}$$

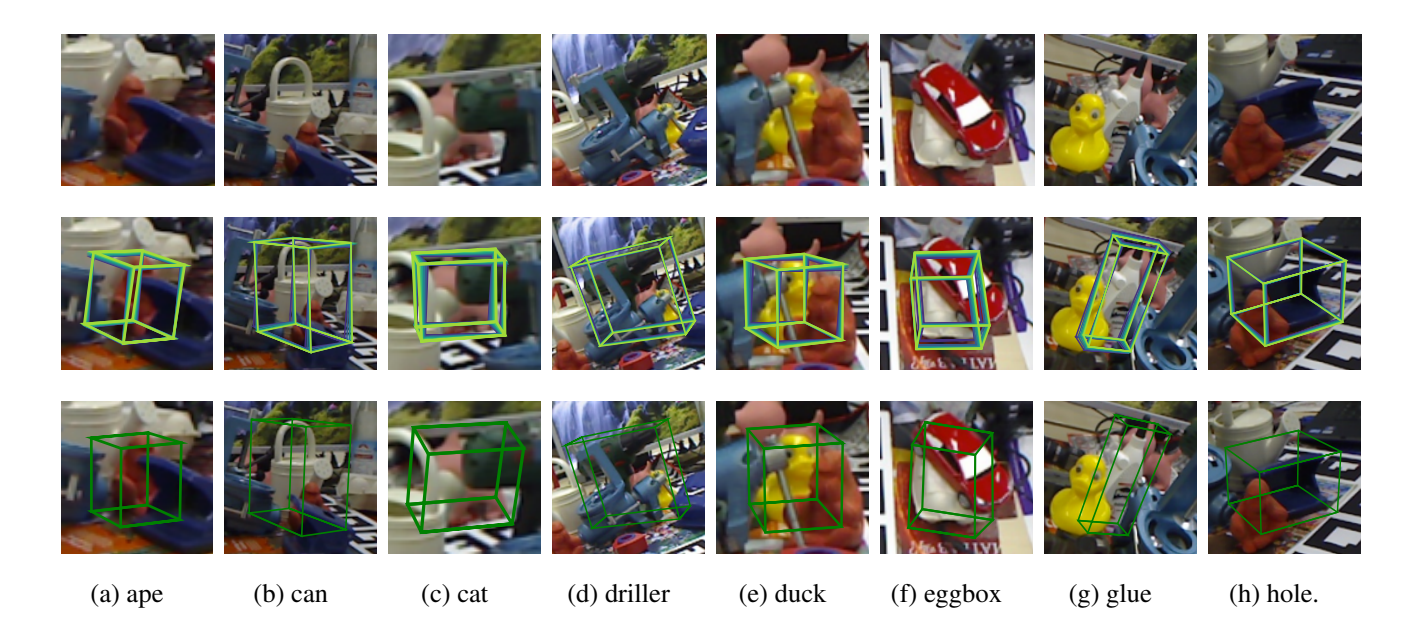


Figure 4: Example results on the Occlusion LineMOD dataset [2]. We show an input RGB image, refined poses, and ground-truth pose from the top to bottom. The color of 3D bounding boxes are changed from purple to lightgreen as optimization progresses.

The minimization of these two loss functions through LM optimization allows our refinement network to learn representations of the input image as well as the rendered object image, which helps in predicting the optimal pose.

$$\mathcal{L} = \mathcal{L}_{ADD(-S)} + \alpha \mathcal{L}_{diff}$$
 (13)

where α is a hyperparameter.

We show the RePOSE framework in Algorithm 1. Note, all the operations inside the LM optimization (Equations (6) and (7)) are differentiable allowing us to learn deep textures \mathcal{C} and Φ using backpropagation.

4. Experiments

4.1. Implementation Details

We train our model using Adam optimizer [11] with a learning rate of 1×10^{-3} , decayed by 0.5 every 100 epochs. The number of channels d in $\mathbf{F}_{\rm inp}$ and $\mathbf{F}_{\rm rend}$ is set to 3 using grid search. The number of iterations t in LM optimization is set to 5. We used pretrained PVNet [17] on the LineMOD and Occlusion LineMOD datasets, and PoseCNN [29] on the YCB-Video [29] dataset as the initial pose estimator Ω . The encoder of U-Net [19] shares its weights with the PVNet and only the weights of the decoder are trained. Following [17], we also add 500 synthetic and fused images for LineMOD and 10K synthetic images for YCB-Video to avoid overfitting during training. In accordance with the convention, to evaluate the scores on the Oc-

```
Algorithm 1: RePOSE Training
```

```
\mathcal{V} = \text{VerticesOf3DModel()};
\mathcal{F} = \text{FACESOF3DModel()};
C = INITIALIZETEXTUREPARAMETERS();
# Iterate over Training Data
for P_{ini}, P_{gt}, I do
       \mathbf{F}_{inp}=UN\text{ET}\left(\mathbf{I}\right);
       \mathbf{P} = \mathbf{P}_{ini};
       for t times do
               \mathbf{F}_{rend} = DEEPTEXTURERENDER(\mathbf{P}, \mathcal{V}, \mathcal{F}, \mathcal{C});
               \mathbf{e} = \text{vec}(\mathbf{F}_{inp}) - \text{vec}(\mathbf{F}_{rend});
               \mathbf{J} = \text{Jacobian}(\mathbf{F}_{\text{rend}}, \mathbf{P}, \mathcal{V});
               \Delta \mathbf{P} = \text{POSEUPDATE}(\mathbf{e}, \mathbf{J}, \mathbf{P});
           \mathbf{P} = \mathbf{P} + \Delta \mathbf{P}; # Update Pose
       \mathbf{P}_{ref} = \mathbf{P};
        \mathcal{L} = \text{Loss}(\mathbf{P}_{\text{ref}}, \mathbf{P}_{\text{gt}}, \mathbf{V});
       UPDATEPARAMETERS(\mathcal{L}, \mathcal{C}, \text{UNET});
```

clusion LineMOD dataset, we use the model trained by only the LineMOD dataset.

4.2. Datasets

All experiments are performed on the LineMOD [9], Occlusion LineMOD [2], and YCB-Video [29] datasets. The LineMOD dataset contains images of small texture-less objects in a cluttered scene under different illumination. High-quality template 3D models of the objects in the images are also provided for render and compare based pose estima-

Table 1: Comparison of RePOSE on Linemod dataset with recent methods including PVNet [17], DPOD [30], HybridPose [23], and EfficientPose [5] using the ADD(-S) score. # of wins denotes in how many categories the method achieves the best score.

Object	[17]	[30]	[23]	[5]	RePOSE
Ape	43.6	87.7	63.1	89.4	79.5
Benchvise	99.9	98.5	99.9	99.7	100
Camera	86.9	96.1	90.4	98.5	99.2
Can	95.5	99.7	98.5	99.7	99.8
Cat	79.3	94.7	89.4	96.2	97.9
Driller	96.4	98.8	98.5	99.5	99.0
Duck	52.6	86.3	65.0	89.2	80.3
Eggbox	99.2	99.9	100	100	100
Glue	95.7	98.7	98.8	100	98.3
Holepuncher	81.9	86.9	89.7	95.7	96.9
Iron	98.9	100	100	99.1	100
Lamp	99.3	96.8	99.5	100	99.8
Phone	92.4	94.7	94.9	98.5	98.9
Average	86.3	95.2	91.3	97.4	96.1
# of wins	0	1	2	6	8

tion. The Occlusion LineMOD dataset is a subset of the LineMOD dataset focused mainly on the occluded objects. We use ADD (-S) [9] score as our evaluation metric.

4.3. Evaluation Metrics

ADD(-S) score. ADD(-S) score [9, 29] is a standard metric which calculates the average distance between objects transformed by the predicted pose $\hat{\mathbf{P}} = \{\hat{\mathbf{R}}, \hat{\mathbf{t}}\}$, and the ground-truth pose $\mathbf{P}_{\text{gt}} = \{\mathbf{R}_{\text{gt}}, \mathbf{t}_{\text{gt}}\}$ using vertices \mathbf{V}_i of the template 3D model \mathcal{M} . The distance is calculated as follows:

$$\frac{1}{N} \sum_{i}^{N} || \left(\hat{\mathbf{R}} \mathbf{V}_{i} + \hat{\mathbf{t}} \right) - \left(\mathbf{R}_{gt} \mathbf{V}_{i} + \mathbf{t}_{gt} \right) || \tag{14}$$

For symmetric objects such as eggbox and glue, we use the following distance metric,

$$\frac{1}{N} \sum_{i=0 \le j \le N}^{N} \min_{0 \le j \le N} || \left(\hat{\mathbf{R}} \mathbf{V}_i + \hat{\mathbf{t}} \right) - \left(\mathbf{R}_{gt} \mathbf{V}_j + \mathbf{t}_{gt} \right) || \quad (15)$$

The predicted pose is considered correct if this distance is smaller than 10% of the target object's diameter. AUC of ADD(-S) computes the area under the curve of the distance used in ADD(-S). The pose predictions with distance larger than 0.1m are not included in computing the AUC. We use AUC of ADD(-S) to evaluate the performance on the YCB-Video dataset [29].

4.4. Quantitative Evaluations

Results on the LineMOD and Occlusion LineMOD datasets. As shown in Tables 1 and 2, RePOSE achieves

Table 2: Comparison of RePOSE on Occlusion LineMOD dataset with recent methods including PVNet [17], DPOD [30], and HybridPose [23] using the ADD(-S) score. Note, we exclude EfficientPose [5] as it is trained on the Occlusion LineMOD dataset. # of wins denotes in how many categories the method achieves the best score.

Object	[17]	[30]*	[23]	RePOSE
Ape	15.8	-	20.9	31.1
Can	63.3	-	75.3	80.0
Cat	16.7	-	24.9	25.6
Driller	65.7	-	70.2	73.1
Duck	25.2	-	27.9	43.0
Eggbox	50.2	-	52.4	51.7
Glue	49.6	-	53.8	54.3
Holepuncher	39.7	-	54.2	53.6
Average	40.8	47.3	47.5	51.6
# of wins	0	-	2	6

the state of the art ADD(-S) scores on the Occlusion LineMOD dataset. In comparison to PVNet [17], RePOSE successfully refines the initial pose estimate in all the object categories, achieving an improvement of 9.8% and 10.8% on the LineMOD and Occlusion LineMOD dataset respectively. On the LineMOD dataset, our score is comparable to the state-of-the art EfficientPose [5] which is slower than RePOSE. The key difference is mainly on the ape and duck categories where our initial pose estimator PVNet [17] performs poorly. Interestingly, for small objects like ape and duck in the Occlusion LineMOD dataset, we show a significant improvement of 10.2 and 15.1 respectively over the prior art HybridPose [23]. RePOSE is also effective on the challening symmetric object categories like eggbox and glue.

Results on the YCB-Video dataset. Table 3 shows the result on the YCB-Video dataset [29]. We also performed experiments using RePOSE as a 6D object tracker using the tracking algorithm proposed in [14]. RePOSE achieves comparable performance with other methods with a 4 times faster runtime of 71 FPS. Further, the result with tracking demonstrates that RePOSE is useful as a real-time 6D object tracker. Note, the scores are heavily affected by the use of synthetic data and various data augmentation [12]. For instance, [12] used one million synthetic images during training, making it hard to compare against fairly.

4.5. Ablation Study

All ablations for RePOSE are conducted on the LineMOD and Occlusion LineMOD datasets using PVNet [17] as an initial pose estimator. We report the results in Tables 4 and 5.

Table 3: Results on the YCB-Video dataset using *RGB only*. The results for DeepIM [14] are computed using the official pre-trained model, and the score inside the parentheses are the reported results from the paper. Refinement FPS denotes FPS of running only a pose refinement network.

Metric	PoseCNN [29]	DeepIM [14]	DeepIM [14]	PVNet [17]	CosyPose [12]	RePOSE	RePOSE w/ track
AUC, ADD(-S)	61.3	74.0	75.5 (81.9)	73.4	84.5	77.2	80.9
ADD(-S)	21.3	43.2	53.6	-	-	49.6	53.1
Refinement FPS	-	22	6	-	12	71	71
#Iterations	-	1	4	-	2	5	5

Table 4: Ablation study of feature representation, feature warping, and a refinement network on the LineMOD dataset. RGB denotes pose refinement using photometric error. FW denotes feature warping after extraction from a CNN or deep texture rendering following first iteration. DPOD denotes using DPOD's refinement network and PVNet as an initial pose estimator. FW, DPOD, and RePOSE are trained with the same dataset, we report the ADD(-S) scores.

Object	PVNet [17]	RGB	CNN w/ FW	DPOD	Ours w/ FW	Ours
Ape	43.6	5.81	65.4	51.2	75.9	79.5
Benchvise	99.9	75.6	99.8	99.5	100	100
Camera	86.9	7.06	96.3	91.1	98.2	99.2
Can	95.5	3.05	99.1	95.7	99.4	99.8
Cat	79.3	3.00	88.6	92.4	92.7	97.9
Driller	96.4	80.9	97.6	98.2	98.7	99
Duck	52.6	0.00	76.2	71.3	84.6	80.3
Eggbox	99.2	8.64	96.4	99.9	100	100
Glue	95.7	5.40	97.2	97.6	98.2	98.3
Holepuncher	81.9	18.7	77.2	89.7	95.1	96.9
Iron	98.9	40.7	98.7	97.9	99.7	100
Lamp	99.3	34.9	91.8	95.5	100	99.8
Phone	92.4	14.6	94.9	97.2	98.7	98.9
Average	86.3	23.0	90.7	90.5	95.5	96.1

Table 5: Ablation study of feature representation, feature warping, and a refinement network on the Occlusion LineMOD dataset. We report the ADD(-S) scores, all other details are same as in Table 4.

Object	PVNet [17]	RGB	CNN w/ FW	DPOD	Our w/ FW	Ours
Ape	15.8	4.96	22.7	22.0	25.8	31.1
Can	63.3	5.22	66.4	71.1	61.3	80.0
Cat	16.7	0.17	11.7	21.9	19.4	25.6
Driller	65.7	61.7	72.1	68.3	71.1	73.1
Duck	25.2	1.80	36.5	30.8	40.8	43.0
Eggbox	50.2	7.75	45.4	42.4	47.7	51.7
Glue	49.6	1.88	45.6	41.3	49.4	54.3
Holepuncher	39.7	21.5	40.8	43.3	40.2	53.6
Average	40.8	13.1	42.9	42.6	44.5	51.6

RGB vs Deep Texture. Instead of using learnable deep textures C, we perform experiments using an original RGB image and rendered image with scanned colors. The inference is all the same except we are using photometric error between two images. The experimental result reported in Tables 4 and 5 show that the ADD(-S) score drops significantly after optimization in all the categories using RGB representation. As illustrated in Figure 5, the LineMOD dataset has three main challenges which makes the pose





(a) Input RGB image

(b) Rendered image

Figure 5: Comparison of object's appearance between an input RGB image and rendered image. Difference of illumination makes pose refinement in RGB space challenging. Furthermore, a left-bottom part of an input RGB image (a) has the same color as the object. This background noise also becomes an obstacle in terms of convergence properties.

refinement using the photometric error difficult — 1) Illumination changes between the input RGB image and synthetic rendering, 2) Poor image gradients due to textureless objects, 3) Background confusion *i.e.* the background color is similar to the object's color.. The ADD(-S) scores drop largely due to these key reasons. On the contrary, RePOSE with learnable deep textures is able to converge within few iterations because of the robustness of deep textures to the above challenges. Tables 4 and 5 clearly demonstrate the effectiveness of our learnable deep textures over using scanned colors for the template 3D model.

CNN with Feature Warping vs Feature Rendering.

Feature warping (FW) is commonly used to minimize photometric or feature-metric error through a non-linear least squares such as Gauss-Newton or Levenberg-Marquardt method. We conduct an experiment to compare a CNN with feature warping and our proposed feature rendering using the deep texture renderer. In a CNN with feature warping, \mathbf{F}_{rend} is extracted in same fashion as the \mathbf{F}_{inp} using a CNN on a normalized synthetic rendering of the template 3D model. This is done just once, following which the feature is warped based on the updated pose at each iteration. The result is shown in Tables 4 and 5. On the LineMOD dataset, we observed on average small improvements by the

feature warping. As the ADD(-S) score only allows the pose estimator to have an mean vertex distance error of 10% of the object's diameter. In this task, this means only 2 to 3 pixel displacement error in 2D image space is allowed especially for small objects. However, it is challenging to train a CNN to extract features with pixel accurate image gradients required for fine-grained pose refinement. On the contrary, our deep feature renderer can compute pixel accurate gradients as the neighborhood vertices on the template 3D model are not strongly correlated. This local constraint is critical for fast and accurate pose refinement.

Comparison with the latest refinement network on the **LineMOD dataset.** We compare our refinement network with the latest fully deep learning-based refinement network proposed in the paper of DPOD [30]. In this experiment, we use the same initial pose estimator [17]. Since DPOD is fully deep learning-based, we increased the amount of the dataset by twice. The refinement network of DPOD outputs a refined pose based on a cropped input RGB image and a synthetic rendering with an initial pose estimate. The experimental result in Tables 4 and 5 shows DPOD fails to refine pose well when trained with the small amount of the dataset. The refinement network of DPOD estimates a refined pose directly and do not consider projective geometry explicitly. This means their network needs to learn not only deep features but also mapping of the deep feature into an object's pose from training data. Several papers [3, 21, 4, 20] report that learning a less complex task can achieve better accuracy and generalization in a 6D camera localization task. Also, we assume the low ADD(-S) score on Occlusion LineMOD dataset implies its low generalization performance to occluded objects. Our network only trains deep features and a refined object's pose is acquired by solving minimization problem based on projective geometry. From this experimental result, the same principle proposed in the field of 6D camera localization is still valid in 6D object pose estimation.

Effect of feature warping. We perform additional experiments to verify the effect of feature warping. To this end, we warp the feature extracted by deep texture renderer based on the updated pose (Ours w/ FW). The result in Table 4 shows that Ours w/ FW achieves 9.2% absolute improvement from PVNet [17] on the LineMOD dataset [9]. However, Table 5 demonstrates the limited ability on the Occlusion LineMOD dataset [2]. From this result, we figure out that warping has an inferior influence on refinement of occluded objects. We conjecture that this difference comes from the fact that warping can not deal with large pose error because unlike our proposed RePOSE, feature warping can only consider the visible surface at the first step. Being different from the methods using feature warping, our iterative deep feature

Table 6: Comparison of number of iterations and refinement runtime. ADD(-S) on the Occlusion LineMOD dataset is reported in this table. Our proposed network is trained by using a pose loss for 5 iterations.

Method	Iteration	ADD(-S) Score	Runtime
AAE [30]	-	-	200 ms
SSD6D [30]	-	-	24 ms
DPOD [30]	-	47.3	5 ms
	0	40.8	0 ms
	1	45.7	6 ms
Ours	2	48.6	8 ms
	3	50.1	10 ms
	4	51.0	12 ms
	5	51.6	14 ms

rendering method can generate a feature with a complete shape. We believe this characteristics of feature rendering leads to successful pose refinement on both datasets.

Number of iteration and run time analysis. Our proposed refinement network, RePOSE can adjust the trade-off between the accuracy and run time by changing the number of iterations. We show the ADD(-S) score and the run time on the Occlusion LineMOD dataset with each iteration count in Table 6. On a machine equipped with Nvidia RTX2080 GPU and Ryzen 7 3700X CPU, our method takes 4 ms for feature extraction of an input RGB image using U-Net and 2 ms per iteration (rendering + pose update through Levenberg-Marquardt optimization [15]). This result shows our method achieves higher performance with the comparable run time with prior art.

5. Conclusion

Real-time pose estimation needs accurate and fast pose refinement. Our proposed method, RePOSE uses efficient deep texture renderer to perform pose refinement at 71 FPS and has practical applications as a real-time 6D object tracker. Our experiments show that learnable deep textures coupled with the efficient non-linear optimization results in accurate 6D object poses. Further, our ablations highlight the fundamental limitations of a convolutional neural network to extract critical information useful for pose refinement. We believe that the concept of using efficient renderers with learnable deep textures instead of a CNN for pose refinement is an important conceptual change and will inspire a new research direction for real-time 6D object pose estimation.

References

 Hatem Said Alismail, Brett Browning, and Simon Lucey. Photometric bundle adjustment for vision-based slam. In ACCV. Springer, May 2016.

- [2] Eric Brachmann, Alexander Krull, Frank Michel, Stefan Gumhold, Jamie Shotton, and Carsten Rother. Learning 6d object pose estimation using 3d object coordinates. In David Fleet, Tomas Pajdla, Bernt Schiele, and Tinne Tuytelaars, editors, *Eur. Conf. Comput. Vis.*, pages 536–551, Cham, 2014. Springer International Publishing. 2, 5, 8, 11
- [3] Eric Brachmann, Alexander Krull, Sebastian Nowozin, Jamie Shotton, Frank Michel, Stefan Gumhold, and Carsten Rother. Dsac - differentiable ransac for camera localization, 2016. 8
- [4] Eric Brachmann and Carsten Rother. Learning less is more - 6d camera localization via 3d surface regression. In *IEEE Conf. Comput. Vis. Pattern Recog.*, June 2018. 8
- [5] Yannick Bukschat and Marcus Vetter. Efficientpose: An efficient, accurate and scalable end-to-end 6d multi object pose estimation approach, 2020. 6
- [6] Bo Chen, Alvaro Parra, Nan Cao, and Tat-Jun Chin. Endto-end learnable geometric vision by backpropagating pnp optimization. In CVPR, 2020. 2
- [7] Guillermo Gallego and Anthony Yezzi. A compact formula for the derivative of a 3-d rotation in exponential coordinates. *Journal of Mathematical Imaging and Vision*, 51:378–384, 03 2015. 10
- [8] P. J. Green. Iteratively reweighted least squares for maximum likelihood estimation, and some robust and resistant alternatives (with discussion). *Journal of the Royal Statistical Society, Series B, Methodological*, 46:149–192, 1984.
- [9] Stefan Hinterstoisser, Vincent Lepetit, Slobodan Ilic, Stefan Holzer, Gary Bradski, Kurt Konolige, and Nassir Navab. Model based training, detection and pose estimation of texture-less 3d objects in heavily cluttered scenes. In ACCV, ACCV'12, page 548–562, Berlin, Heidelberg, 2012. Springer-Verlag. 2, 5, 6, 8, 10, 11
- [10] Wadim Kehl, Fabian Manhardt, Federico Tombari, Slobodan Ilic, and Nassir Navab. Ssd-6d: Making rgb-based 3d detection and 6d pose estimation great again. In *Int. Conf. Comput. Vis.*, 2017. 1, 2
- [11] Diederik P. Kingma and Jimmy Ba. Adam: A method for stochastic optimization. In Yoshua Bengio and Yann LeCun, editors, *Int. Conf. Learn. Represent.*, 2015. 5
- [12] Y. Labbe, J. Carpentier, M. Aubry, and J. Sivic. Cosypose: Consistent multi-view multi-object 6d pose estimation. In *Eur. Conf. Comput. Vis.*, 2020. 2, 6, 7, 10, 11
- [13] Vincent Lepetit, Francesc Moreno-Noguer, and Pascal Fua. Epnp: An accurate o(n) solution to the pnp problem. *Int. J. Comput. Vision*, 81(2):155–166, Feb. 2009.
- [14] Yi Li, Gu Wang, Xiangyang Ji, Yu Xiang, and Dieter Fox. Deepim: Deep iterative matching for 6d pose estimation. In Eur. Conf. Comput. Vis., 2018. 1, 2, 6, 7, 10, 11
- [15] Jorge J. Moré. The levenberg-marquardt algorithm: Implementation and theory. In G. A. Watson, editor, *Numerical Analysis*, pages 105–116, Berlin, Heidelberg, 1978. Springer Berlin Heidelberg. 2, 3, 8
- [16] R. Mur-Artal, J. M. M. Montiel, and J. D. Tardós. Orb-slam: A versatile and accurate monocular slam system. *IEEE Transactions on Robotics*, 31(5):1147–1163, 2015.

- [17] Sida Peng, Xiaowei Liu, and Hujun Bao. Pvnet: Pixel-wise voting network for 6dof pose estimation. In *IEEE Conf. Comput. Vis. Pattern Recog.*, 2019. 1, 2, 3, 5, 6, 7, 8, 11
- [18] Mahdi Rad and Vincent Lepetit. BB8: A scalable, accurate, robust to partial occlusion method for predicting the 3d poses of challenging objects without using depth. CoRR, abs/1703.10896, 2017. 2
- [19] O. Ronneberger, P.Fischer, and T. Brox. U-net: Convolutional networks for biomedical image segmentation. In *MIC-CAI*, volume 9351 of *LNCS*, pages 234–241. Springer, 2015. (available on arXiv:1505.04597 [cs.CV]). 3, 5
- [20] Torsten Sattler, B. Leibe, and L. Kobbelt. Efficient & effective prioritized matching for large-scale image-based localization. *IEEE Trans. Pattern Anal. Mach. Intell.*, 39:1744–1756, 2017. 8
- [21] Torsten Sattler, Qunjie Zhou, Marc Pollefeys, and Laura Leal-Taixe. Understanding the limitations of cnn-based absolute camera pose regression. In *IEEE Conf. Comput. Vis.* Pattern Recog., June 2019. 8
- [22] J. L. Schönberger and J. Frahm. Structure-from-motion revisited. In *IEEE Conf. Comput. Vis. Pattern Recog.*, pages 4104–4113, 2016.
- [23] Jiaru Song and Qixing Huang. Hybridpose: 6d object pose estimation under hybrid representations. In *IEEE Conf. Com*put. Vis. Pattern Recog., 2020. 1, 2, 6
- [24] Martin Sundermeyer, Zoltan-Csaba Marton, Maximilian Durner, Manuel Brucker, and Rudolph Triebel. Implicit 3d orientation learning for 6d object detection from rgb images. In Eur. Conf. Comput. Vis., 2018. 2
- [25] Chengzhou Tang and Ping Tan. BA-Net: Dense Bundle Adjustment Network. 2019. 2, 3
- [26] Jonathan Tremblay, Thang To, Balakumar Sundaralingam, Yu Xiang, Dieter Fox, and Stan Birchfield. Deep object pose estimation for semantic robotic grasping of household objects. 2018. 2
- [27] L. von Stumberg, P. Wenzel, Q. Khan, and D. Cremers. Gnnet: The gauss-newton loss for multi-weather relocalization. 5(2):890–897, 2020. 2
- [28] Angtian Wang, Adam Kortylewski, and Alan Yuille. Nemo: Neural mesh models of contrastive features for robust 3d pose estimation, 2021. 2
- [29] Yu Xiang, Tanner Schmidt, Venkatraman Narayanan, and Dieter Fox. Posecnn: A convolutional neural network for 6d object pose estimation in cluttered scenes. 2018. 2, 3, 5, 6, 7
- [30] Sergey Zakharov, Ivan Shugurov, and Slobodan Ilic. Dpod: 6d pose object detector and refiner. In *Int. Conf. Comput. Vis.*, 2019. 1, 2, 6, 8
- [31] Zhengyou Zhang. Iterative Closest Point (ICP), pages 433–434. Springer US, Boston, MA, 2014. 2

A. Derivation of Camera Jacobian Matrix

Notation: $\mathbf{R} \in \mathrm{SO}(3)$ denotes a rotation matrix, $\mathbf{t} \in \mathbb{R}^3$ denotes a translation vector, $\mathbf{w} \in \mathfrak{so}(3)$ denotes a rotation vector, $\mathbf{P} = (\mathbf{w} \ \mathbf{t}) \in \mathbb{R}^6$ is a pose representation using a rotation and translation vector, f_x and f_y are focal lengths, p_x and p_y are the principal point offsets, \mathbf{X} and \mathbf{x} denote a homogeneous and inhomogeneous 2D image coordinate, subscript w, c denotes a coordinate is defined in the world, and camera coordinate system respectively, and $\mathbf{Id} \in \mathbb{R}^{3\times3}$ is an 3×3 identity matrix. \mathbf{R} and \mathbf{w} represents the same rotation.

Derivation: Jacobian matrix \mathbf{J} of the objective function with respect to a pose \mathbf{P} is required to perform deep feature-based pose optimization. We show the detailed derivation of a camera jacobian matrix $\frac{\partial \mathbf{x}}{\partial \mathbf{P}}$ at each pixel in Equation 9. The camera jacobian matrix can be decomposed more as follows;

$$\frac{\partial \mathbf{x}}{\partial \mathbf{P}} = \begin{pmatrix} \frac{\partial \mathbf{R}}{\partial \mathbf{w}} \frac{\partial \mathbf{x}}{\partial \mathbf{R}} \\ \frac{\partial \mathbf{x}}{\partial \mathbf{t}} \end{pmatrix} \in \mathbb{R}^{6 \times 2}$$
 (16)

Using the derivative calculation method of a rotation matrix with respect to a rotation vector proposed in [7], the following equation is acquired.

$$\frac{\partial \mathbf{R}}{\partial \mathbf{w}} = \left(\frac{\partial \mathbf{R}}{\partial w_{1}} \quad \frac{\partial \mathbf{R}}{\partial w_{2}} \quad \frac{\partial \mathbf{R}}{\partial w_{3}}\right)^{T}$$

$$= \begin{pmatrix} vec\left(\frac{w_{1}[\mathbf{w}]_{\times} + [\mathbf{w} \times (\mathbf{Id} - \mathbf{R})\mathbf{e}_{1}]_{\times}}{\|\mathbf{w}\|^{2}}\mathbf{R}\right) \\ vec\left(\frac{w_{2}[\mathbf{w}]_{\times} + [\mathbf{w} \times (\mathbf{Id} - \mathbf{R})\mathbf{e}_{2}]_{\times}}{\|\mathbf{w}\|^{2}}\mathbf{R}\right) \\ vec\left(\frac{w_{3}[\mathbf{w}]_{\times} + [\mathbf{w} \times (\mathbf{Id} - \mathbf{R})\mathbf{e}_{3}]_{\times}}{\|\mathbf{w}\|^{2}}\mathbf{R}\right) \\ \end{pmatrix} \in \mathbb{R}^{3 \times 9}$$
(17)

where *vec* is a vectorize operation, $[\mathbf{x}]_{\times}$ is a conversion from a 3-d vector to a skew-symmetric matrix, \mathbf{e}_i is a *i*th 3-d basis vector. \mathbf{R} is regarded as a 9-d vector for simplicity. A camera and image coordinate \mathbf{x}_c and \mathbf{x} can be calculated as follows;

$$\mathbf{x}_c = \mathbf{R}\mathbf{x}_w + \mathbf{t} \tag{18}$$

$$\mathbf{x} = \begin{pmatrix} \frac{f_x x_c}{z_c} + p_x \\ \frac{f_y y_c}{z_c} + p_y \end{pmatrix}$$
 (19)

Using Equations (18) and (19), the following derivatives can be obtained.

$$\frac{\partial \mathbf{x}}{\partial \mathbf{R}} = \begin{pmatrix}
\frac{f_x x_w}{z_c} & 0 \\
\frac{f_x y_w}{z_c} & 0 \\
0 & \frac{f_y x_w}{z_c} \\
0 & \frac{f_y y_w}{z_c} \\
-\frac{f_y y_w}{z_c} \\
-\frac{f_x x_c x_w}{z_c} & -\frac{f_y y_c x_w}{z_c^2} \\
-\frac{f_x x_c y_w}{z_c^2} & -\frac{f_y y_c y_w}{z_c^2} \\
-\frac{f_x x_c z_w}{z_c^2} & -\frac{f_y y_c z_w}{z_c^2} \\
-\frac{f_x x_c z_w}{z_c^2} & -\frac{f_y y_c z_w}{z_c^2}
\end{pmatrix}$$
(20)

$$\frac{\partial \mathbf{x}}{\partial \mathbf{t}} = \begin{pmatrix} \frac{f_x}{z_c} & 0\\ 0 & \frac{f_y}{z_c}\\ -\frac{f_x x_c}{z_c^2} & -\frac{f_y y_c}{z_c^2} \end{pmatrix} \in \mathbb{R}^{3 \times 2}$$
(21)

B. Additional Ablation Study

Ablation on effect of warping. We show the median of absolute angular and relative translation error on the LineMOD and Occlusion LineMOD datasets in Tables 7 and 8. The relative translation error is computed with respect to object diameter. The initial pose error on the LineMOD dataset [9] is relatively small and the methods using warping improve score properly. On the contrary, the initial pose error is large on the Occlusion LineMOD dataset. In that case, feature warping becomes less effective. Being different from the methods using feature warping, our iterative deep feature rendering method can generate a feature with a complete shape. We believe this characteristics of feature rendering leads to successful reduction of the error of rotation and translation on both datasets.

Runtime Ablation on Feature Warping. DeepIM [14] and CosyPose [12] run a CNN every iteration on a concatenated image of a zoomed input and rendered images to compare these two images and output a pose directly. According to the ablation study by [14], high-resolution zoom-in is a key and it improves the ADD(-S) score by 23.4. However, as shown in Table 9, extracting image features from zoomed

Table 7: Comparison of the median of absolute angular and relative translation error on the LindMOD dataset [9]. We do not report the rotation error of symmetric objects (eggbox, and glue) because of its non-unique rotation representation.

Object	PVN	Vet [17]	CNN	w/FW	Ours	w/ FW	(Ours
	Rotation	Translation	Rotation	Translation	Rotation	Translation	Rotation	Translation
Ape	2.213°	0.119	1.849°	0.069	1.446°	0.055	1.197°	0.051
Benchvise	1.030°	0.022	0.857°	0.022	0.644°	0.014	0.757°	0.010
Cam	1.183°	0.045	0.896°	0.030	1.322°	0.073	0.713°	0.023
Can	0.958°	0.032	1.238°	0.033	0.995°	0.040	0.674°	0.017
Cat	1.260°	0.050	1.177°	0.041	0.941°	0.036	0.857°	0.035
Driller	1.008°	0.029	0.812°	0.023	1.057°	0.060	0.773°	0.014
Duck	1.701°	0.078	1.701°	0.055	1.531°	0.042	1.481°	0.053
Eggbox	-	0.056	-	0.074	-	0.048	-	0.025
Glue	-	0.050	-	0.049	-	0.040	-	0.036
Holepuncher	1.265°	0.052	1.548°	0.058	1.295°	0.060	1.009°	0.029
Iron	1.205°	0.027	1.223°	0.027	0.927°	0.020	0.911°	0.015
Lamp	1.050°	0.029	1.235°	0.042	1.054°	0.019	0.902°	0.020
Phone	1.208°	0.040	1.122°	0.032	0.925°	0.019	0.889°	0.025
Average	1.280°	0.048	1.242°	0.043	1.103°	0.040	0.924°	0.027

Table 8: Comparison of the median of absolute angular and relative translation error on the Occlusion LindMOD dataset [2]. We do not report the rotation error of symmetric objects (eggbox, and glue) because of its non-unique rotation representation.

Object	PVN	let [17]	CNN	w/FW	Ours	w/ FW	(Durs
	Rotation	Translation	Rotation	Translation	Rotation	Translation	Rotation	Translation
Ape	4.103°	0.210	4.222°	0.185	4.015°	0.171	3.871°	0.157
Can	2.722°	0.068	2.879°	0.069	2.793°	0.067	2.704°	0.043
Cat	6.012°	0.239	6.480°	0.363	6.552°	0.335	5.852°	0.274
Driller	2.774°	0.072	2.567°	0.131	2.762°	0.120	2.545°	0.056
Duck	6.923°	0.156	6.795°	0.115	6.537°	0.108	6.533°	0.102
Eggbox	-	0.325	-	0.295	-	0.284	-	0.318
Glue	-	0.275	-	0.246	_	0.235	_	0.266
Holepuncher	3.969°	0.121	3.917°	0.116	3.918°	0.126	3.629°	0.088
Average	4.417°	0.183	4.477°	0.190	4.430°	0.181	4.189°	0.163

Table 9: Runtime comparison among recent methods. In CNN with feature warping (FW) the initial feature is obtained using CNN and then warp the feature based on an updated pose. We assume the number of iterations is 5 for RePOSE and FW denotes feature warping.

Method	Runtime
DeepIM [14] (4 iters)	161 ms
CosyPose [12] (2 iters)	83 ms
RePOSE w/ different fea	ture extraction methods
CNN w/ FW	22 ms
Ours w/ FW	19 ms
Ours w/o FW	14 ms

resolution (no zoom-in is required). Additionally, an image representation of a rendered image can be extracted within 1ms because of deep texture rendering. This makes the runtime of RePOSE faster than prior methods while keeping a comparable accuracy to the prior methods. We also measure the runtime of RePOSE using different feature extraction methods for a rendered image. As shown in Table 9 in the supplemental and Table 4 and 5 in the main paper, RePOSE using feature warping achieves the fastest (14ms) and highest accuracy among these three variants.

images multiple times leads to a slow runtime. Instead, Re-POSE runs a CNN once for an input image with the original